Hydrogen Silsesquioxane: A Molecular Precursor for Nanocrystalline Si−SiO_2 Composites and Freestanding Hydride-Surface-Terminated Silicon Nanoparticles

Colin M. Hessel, Eric J. Henderson, and Jonathan G. C. Veinot*

Department of Chemistry, University of Alberta, Edmonton, Alberta, Canada

Received February 3, 2006. Revised Manuscript Received August 28, 2006

We report the bulk preparation of nanocrystalline Si−SiO_2 (*nc*-Si/SiO_2) composites via straightforward reductive thermal annealing of a well-defined molecular precursor, hydrogen silsesquioxane. The presented method affords quantitative yields of composite powders in large quantities. Freestanding, hydride-surface-terminated silicon nanocrystals that photoluminesce throughout the visible spectrum are readily liberated from *nc*-Si/SiO_2 composite powders upon etching in ethanol−water solutions of hydrofluoric acid. Composites and freestanding particles were characterized using transmission electron microscopy (TEM), selected area electron diffraction (SAED), X-ray powder diffraction (XRD), X-ray photoelectron spectroscopy (XPS), photoluminescence (PL) spectroscopy, Fourier transform infrared spectroscopy (FT−IR), and thermogravimetric analysis (TGA).

1. Introduction

Silicon nanostructures including porous silicon (p-Si),[1] silicon rich oxides (SROs),[2] and freestanding Si nanoparticles (FS-*nc*-Si)[3] have been the focus of intense research because of their unique chemical and optical characteristics. The electronic structure of bulk silicon provides an indirect band gap of 1.12 eV, with the lowest point of the conduction band and the highest point of the valence band occurring at different coordinates in reciprocal space. This makes the band gap optical transition dipole-forbidden and limits practical optoelectronic application of bulk silicon because of low photoluminescence intensity and slow carrier dynamics (i.e., long-lived excited states). As the dimensions of a semiconductor particle approach the radius of an exciton in the bulk material (ca. 5 nm for Si), the band gap energy increases and pseudo-continuous bands become discrete energy levels that are populated according to quantum mechanical selection rules. Consequently, quantum confinement effects emerge and photoluminescence blue shifts with decreasing particle size and increases in intensity.[4] Some researchers suggest that the photoluminescence (PL) observed from photoexcited Si nanoparticles arises because the band gap transition becomes weakly dipole-allowed in this quantum confined size regime.[5] Others claim photoemission originates from the passivation of surface traps present in bulk Si.[6] Regardless of the explanation, a characteristic photoemission maximum at approximately 1.7 eV is seen for many Si-based nanostructures, including the "Si quantum wires" reported by Canham,[7] nanocrystalline *nc*-Si/SiO_2 composites,[2] and freestanding Si nanoparticles prepared via solution,[8−10] precursor pyrolysis,[11,12] and physical techniques.[13−15] The unique optical properties and electrochemical stability[16] of nanoscale elemental Si offer significant potential for a variety of light emission applications. Furthermore, the biocompatibility of Si and SiO_2 makes these materials potentially useful in sensing applications where toxic,[17] electrochemically active compound semiconductor nanoparticles are impractical.

Measuring the direct effect of Si nanocrystal size on the PL spectrum of Si/SiO_2 composites and freestanding Si nanocrystals appears complicated, with interface effects, surface chemistry, and particle interactions[18] playing key roles. This complexity is well-illustrated by the optical response of ultrasmall Si particles ($d \approx 1.1-1.4$ nm).[19] The experimental optical behavior of hydride-surface-terminated FS-*nc*-Si of this size is dominated by blue emission, and reports suggest either a direct or indirect gap transition.[20,21] This is very different from observations previously noted

* Corresponding author. Fax: 780-492-8231. Tel: 780-492-720. E-mail: jveinot@ualberta.ca.

(1) Buriak, J. M. *Chem. Rev.* **2002**, *102*, 1271.
(2) Meldrum, A. *Recent Res. Dev. Nucl. Phys.* **2004**, *1*, 93.
(3) Veinot, J. G. C. *Chem. Commun.* **2006**, DOI:10.1039/b607476f.
(4) Bulk Si exhibits a sharp emission line at 1060 nm when cooled to liquid helium temperatures.
(5) Takagahara, T.; Takeda, K. *Phys. Rev. B* **1992**, *46*, 15578.
(6) Klimov, V. I.; Schwarz, C. J.; McBranch, D. W.; White, C. W. *Appl. Phys. Lett.* **1998**, *73*, 2603.
(7) Canham, L. T. *Appl. Phys. Lett.* **1990**, *57*, 1046.
(8) Baldwin, R. K.; Pettigrew, K. A.; Garno, J. C.; Power, P. P.; Liu, G.-Y.; Kauzlarich, S. M. *J. Am. Chem. Soc.* **2002**, *124*, 1150.
(9) Pettigrew, K.; Liu, Q.; Power, P. P.; Kauzlarich, S. M. *Chem. Mater.* **2003**, *15*, 4005.
(10) Rowsell, B. D.; Veinot, J. G. C. *Nanotechnology* **2005**, *16*, 732.
(11) Li, X. G.; He, Y. Q.; Swihart, M. T. *Langmuir* **2004**, *20*, 4720.
(12) Li, X. G.; He, Y. Q.; Talukdar, S. S.; Swihart, M. T. *Langmuir* **2003**, *19*, 8490.
(13) Nayfeh, M. H.; Barry, N.; Therrien, J.; Akcakir, O.; Gratton, E.; Belomoin, G. *Appl. Phys. Lett.* **2001**, *78*, 1131.
(14) Nayfeh, M. H.; Akcakir, O.; Belomoin, G.; Barry, N.; Therrien, J.; Gratton, E. *Appl. Phys. Lett.* **2000**, *77*, 4086.
(15) Belomoin, G.; Therrien, J.; Smith, A.; Rao, S.; Twesten, R.; Chaleb, S.; Nayfeh, M. H.; Wagner, L.; Mitas, L. *Appl. Phys. Lett.* **2002**, *80*, 841.
(16) Ding, Z.; Quinn, B. M.; Haram, S. K.; Pell, L. E.; Korgel, B. A.; Bard, A. J. *Science* **2002**, *296*, 1293.
(17) Derfus, A. M.; Chan, W. C. W.; Bhatia, S. N. *Nano Lett.* **2004**, *4*, 11
(18) Glover, M.; Meldrum, A. *Opt. Mater.* **2005**, *27*, 977.
(19) Zhou, Z.; Brus, L.; Friesner, R. *Nano Lett.* **2003**, *3*, 163−167.

10.1021/cm0602803 CCC: $33.50
Published on Web 12/06/2006

for oxide-terminated particles of equivalent size that show a red-yellow emission resulting from an indirect gap transition.[22] Very similar observations were reported by Wolkin et al. for blue-emitting, hydride-surface-terminated nanocrystals in p-Si, whose PL maximum red-shifted upon oxidation.[23] These data appear to contradict simple quantum confinement because the decrease in Si particle core size resulting from oxidation seems to cause the PL maximum to decrease in energy. To aid in our understanding of these complex optical properties, diverse methods for relating PL energy maxima to particle size have been proposed, including the effective mass approximation,[24] empirical tight binding band theory,[25,26] empirical pseudopotential approximation,[27,28] and ab initio local density approximation.[29,30] Still, the size effects and the influence of the indirect band gap of bulk Si on the PL behavior of Si nanocrystals remains the subject of much controversy and scientific curiosity.

To facilitate better understanding of FS-*nc*-Si optical and chemical response, straightforward, cost-effective, scalable methods for preparing materials of controlled polydispersity, size, crystal structure, and surface chemistry are necessary. Well-established physical techniques for preparing Si nanostructures often employ highly corrosive reagents (e.g., hydrofluoric acid) and specialized, highly technical procedures (e.g., ion implantation,[31,32] vacuum evaporation,[33] sputtering,[34] and laser ablation[35]). Whereas freestanding particles have been dislodged from p-Si surfaces,[36] published data suggest individual Si nanoparticles remain trapped in larger (i.e., $\geq 1\ \mu$m) pieces of the p-Si structure and that these methods are impractical for preparing macroscopic sample sizes (ca. >500 mg).[13−15] Similar particle liberation protocols and bulk preparation of Si nanoparticles from traditional thin film SRO matrices are impractical given extremely small sample sizes.[37] To this end, a series of methods have been introduced for preparing FS-*nc*-Si. Laser-induced precursor pyrolysis has recently been reported as an efficient method for preparing large quantities of Si nanoparticles from silane at rates of 20−200 mg/h. This approach relies on specialized laser equipment and custom designed reactors not available in most synthetic laboratories.[11,12] Solution-based procedures[10,38−45] provide some postsynthesis material processability, but are often plagued by wide size distributions, specialized reagents, small sample sizes, material purity, ill-defined particle surface chemistry, and limited ambient stability—all criteria crucial to the eventual application of these materials.

SROs remain a promising class of nanostructured materials composed of luminescent, crystalline Si nanoparticles embedded in an environmentally inert SiO_2-like matrix. To date, one major limitation to their application in the synthesis of FS-*nc*-Si has been limited sample size (vide supra). One common method for preparing SROs employs a multistep process; the first stage involves deposition of thin "SiO" precursor films using physical methods such as vapor deposition, physical sputtering, or e-beam evaporation to deposit films onto flat substrates.[2] These recipe-based approaches control the Si:O ratio by maintaining a specific oxygen flow rate (i.e., partial pressure) during reactive deposition of "SiO" or by controlling the co-deposition rates of Si, "SiO", and SiO_2 to produce SiO_x films ($0 \leq x \leq 2$).[46] Films are subsequently annealed at high temperature in a reducing atmosphere (typically 4% H_2, 96% inert gas) to promote the formation of Si nanocrystals.[47] Iterative variation of experimental parameters and postdeposition microprobe analyses have previously shown that precursor films with compositional ratios up to 1.0:1.5 Si:O produce PL characteristic of *nc*-Si upon annealing at ca. 1100 °C. Still, fundamental questions remain regarding the mechanism for nanoparticle formation, the relationship between Si particle size and peak PL energy, among others.[2] Unfortunately, the exact composition, structure, and purity of "SiO" are the subject of a longstanding controversy[48−50] and are strongly dependent upon processing conditions.[48] Further, the exact chemical structure of "SiO_x" remains largely ill-defined.[51]

(20) (a) Warner, J. H.; Rubinsztein-Dunlop, H.; Tilley, R. D. *J. Phys. Chem. B* **2005**, *109*, 19064−19067. (b) Warner, J. H.; Hoshino, A.; Yamamoto, K.; Tilley, R. D. *Angew. Chem., Int. Ed.* **2005**, *44*, 4550−4554. (c) Tilley, R. D.; Warner, J. H.; Yamamoto, K.; Matsui, I.; Fujimori, H. *Chem. Commun.* **2005**, 1833−1835.
(21) Holmes, J. D.; Ziegler, K. J.; Doty, R. C.; Pell, L. E.; Johnston, K. P.; Korgel, B. A. *J. Am. Chem. Soc.* **2001**, *123*, 3743−3748.
(22) a) Brus, L. *J. Phys. Chem.* **1994**, *98*, 3575−3581. (b) Littau, K. A.; Szajowski, P. J.; Muller, A. J.; Kortan, A. R.; Brus, L. E. *J. Phys. Chem.* **1993**, *97*, 1224−1230.
(23) Wolkin, M. V.; Jorne, J.; Fauchet, P. M.; Allan G.; Delerue, C. *Phys. Rev. Lett.* **1999**, *82*, 197−200.
(24) Breitenecker, M.; Sexl, R.; Thirring, W. *Z. Phys.* **1964**, *182*, 123.
(25) Hill, N. A.; Whaley, K. B. *J. Electron. Mater.* **1996**, *25*, 269.
(26) Hill, N. A.; Whaley, K. B. *Phys. Rev. Lett.* **1995**, *75*, 1130.
(27) Wang, L. W.; Zunger, A. *J. Phys. Chem.* **1994**, *98*, 2158.
(28) Delerue, C.; Allan, G.; Lannoo, M. *Phys. Rev. B* **1993**, *48*, 11024.
(29) Delerue, C.; Allan, G.; Lannoo, M. *J. Lumin.* **1998**, *80*, 65.
(30) Ogut, S.; Chelikowsky, J. R.; Louie, S. G. *Phys. Rev. Lett.* **1997**, *79*, 1770.
(31) Shimizu-Iwayama, T.; Ohshima, M.; Niimi, T.; Nakao, S.; Saitoh, K.; Fujita, T.; Itoh, N. *J. Phys. Condens. Matter* **1993**, *5*, L375.
(32) Meldrum, A.; Haglund, R. F.; Boatner, L. A.; White, C. W. *Adv. Mater.* **2001**, *13*, 1431.
(33) Kahler, U.; Hofmeister, H. *Opt. Mater.* **2001**, *17*, 83.
(34) Gorbilleau, F.; Portier, X.; Ternon, C.; Voivenel, P.; Madelon, R.; Riszk, R. *Appl. Phys. Lett.* **2001**, *78*, 3058.
(35) Orii, T.; Hirasawa, M.; Seto, T. *Appl. Phys. Lett.* **2003**, *83*, 3395.
(36) Valenta, J.; Janda, P.; Dohnalova, K.; Niznansky, D.; Vacha, F.; Linnros, J. *Opt. Mater.* **2005**, *27*, 1046.
(37) Recently, bulk thermolysis of "SiO_x" was reported; however, no yield was provided. See: Liu, S. M.; Sato, S.; Kimura, K. *Langmuir* **2005**, *21*, 6324.
(38) Heath, J. R.; Shiang, J. J.; Alivisatos, A. P. *J. Chem. Phys.* **1994**, *101*, 1607.
(39) Baldwin, R. K.; Pettigrew, K. A.; Garno, J. C.; Power, P. P.; Liu, G. Y.; Kauzlarich, S. M. *J. Am. Chem. Soc.* **2002**, *124*, 1150.
(40) Zou, J.; Baldwin, R. K.; Pettigrew, K. A.; Kauzlarich, S. M. *Nano Lett.* **2004**, *7*, 1181.
(41) Pettigrew, K. A.; Liu, Q.; Power, P. P.; Kauzlarich, S. M. *Chem. Mater.* **2003**, *15*, 4005.
(42) Liu, Q.; Kauzlarich, S. M. *Mater. Sci. Eng., B* **2002**, *96*, 72.
(43) Mayeri, D.; Phillips, B. L.; Augustine, M. P., Kauzlarich, S. M. *Chem. Mater.* **2001**, *13*, 765.
(44) Baldwin, R. K.; Pettigrew, K. A.; Ratai, E.; Augustine, M. P.; Kauzlarich, S. M. *Chem. Commun.* **2002**, *17*, 1822.
(45) Wilcoxon, J. P.; Provencio, P. P.; Samara, G. A. *Phys. Rev. B* **1999**, *60*, 2704.
(46) Meldrum, A.; Hryciw, A.; MacDonald, A. N.; Blois, C.; Marsh, K.; Wang, J.; Li, Q. *J. Vac. Sci. Technol.* **2006**, in press.
(47) Neufeld, E.; Wang, S.; Aptez, R.; Buchal, Ch.; Carius, R.; White, C. W.; Thomas, D. K. *Thin Solid Films* **1997**, *294*, 238.
(48) Holhl, A.; Weider, T.; van Aken, P. A.; Weirich, T.-E.; Denninger, G.; Vidal, M.; Oswald, S.; Deneke, C.; Mayer, J.; Fuess, H. *J. Non-Cryst. Solids* **2003**, *320*, 255 and references therein.
(49) Schulmeister, K.; Mader, W. *J. Non-Cryst. Solids* **2003**, *320*, 143.
(50) Commercially available "SiO" is an orange/brown/black solid; however, SiO is reported to be a white, crystalline (cub.) solid with mp > 1702 °C. See: *Handbook of Chemistry and Physics*, 73rd ed.; Linde, D. R., Ed.; CRC Press: Boca Raton, FL, 1997.

Scheme 1. Thermal Processing of Hydrogen Silsesquioxane (HSQ) for Preparing Silicon Nanoparticle/SiO_2-like (*nc*-Si/SiO_2) Nanocomposites

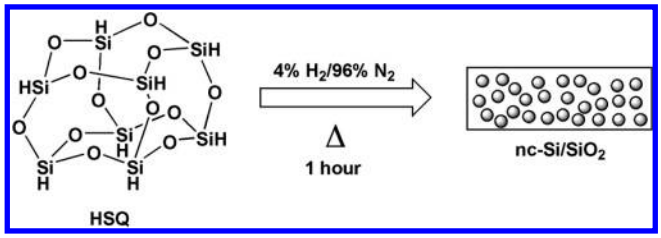

These uncertainties potentially hinder the rational study of chemical composition and its influence on the material properties of SRO nanoparticle composites.

Silsesquioxanes are commercially available, solution processable, discrete, structurally well-defined molecules composed of silicon−oxygen frameworks with empirical formulas ($RSiO_{1.5}$) in which R may be a variety of chemical functionalities (e.g., H, alkyl, silyl, and aromatic). The chemistry of these compounds is well-established, and a variety of cage structures are known.[52] Hydrogen silsesquioxane (HSQ, Scheme 1), a totally inorganic silsesquioxane ($H_8Si_8O_{12}$), is one of the most widely studied and has been investigated as a model silica surface,[53−56] luminescent material,[57] and a catalytic support.[58,59] Examples of high purity silica have also been prepared from silsesquioxane precursors.[60] It is generally accepted that upon oxidative thermal curing, the silsesquioxane cage structure of HSQ collapses to release SiH_4[61] and a SiO_2-like network solid forms whose dielectric,[62] mechanical, and processing characteristics depend on the curing conditions. Dielectric films produced by thermal curing of HSQ currently find application as spin-on, planarizing dielectric interlayers in the microchip industry.[62] To date, no Si nanoparticle preparation employing silsesquioxanes has been reported. The similar composition (i.e., $Si_{1.0}$:$O_{1.5}$) and thermodynamic instability of both HSQ and the "ideal" SiO_x precursor films suggest HSQ may be a suitable molecular precursor to *nc*-Si/SiO_2 composites upon reductive thermal curing. In addition, the structural tunability of HSQ should offer control over film composition and structure previously unattainable using existing physical methods for SiO_x film preparation. Here, we report the application of HSQ as a molecular precursor for the straightforward large scale (ca. 0.25 g) synthesis of *nc*-Si/SiO_2-like nanocomposites and the corresponding liberation of freestanding Si nanocrystals that photoluminesce throughout the visible spectrum.

2. Experimental Details

Reagents and Materials. HSQ was purchased from Dow Corning (tradename FOx-12) as a 10 wt % solution in methyl isobutyl ketone. This stock solution was used as received and stored in subdued light and inert atmosphere prior to use. Electronic grade hydrofluoric acid (49% aqueous solution, J. T. Baker), HPLC grade pentane (Caledon Laboratory Chemicals), and reagent grade ethanol (95%, Sigma-Aldrich) were used as received. High-purity water (18.2 MΩ/cm) was obtained from a Barnstead Nanopure Diamond purification system.

Bulk *nc*-Si/SiO_2 Composite Preparation (1−8). Solvent was removed from the HSQ stock solution. The resulting white solid was placed in a quartz crucible and transferred in an inert atmosphere to a high-temperature furnace and annealed for 1 h in a 4% H_2 and 96% N_2 atmosphere. In the furnace, HSQ samples were heated at 20 °C/min until the desired peak temperature was reached, at which time the samples remained at 500, 600, 700, 800, 900, 1000, or 1100 °C for 1 h. After cooling to room temperature, the darkened solid was removed and mechanically ground in a mortar and pestle to yield a fine powder whose color varied with processing temperature (see Figure 1 and Table 1). To increase particle size uniformity and facilitate more efficient etching, we shook the powder with glass beads using a wrist action shaker, suspended it in distilled water, and collected it by vacuum filtration with Whatman #2 filter paper. The product yields depend slightly on processing temperature and are summarized in Table 1. The resulting powders were evaluated using XRD.

Liberation of Hydride-Surface-Terminated FS-*nc*-Si (9−13). A representative etching procedure involves transferring 0.3 g of the ground **7** to a Teflon beaker containing 10 mL of a 1:1:1 49% HF:H_2O:ethanol solution. The mixture is stirred for 1.5 h to remove the silica matrix, yielding 0.03 g of **10** as a yellow powder. Once liberated, the hydrophobic, hydride-terminated Si crystals are extracted into two 5 mL portions of pentane and kept under an inert atmosphere. Etching parameters for **9**−**13** are summarized in Table 2. This etching procedure is fully scalable.

Thermogravimetric Analysis. Thermogravimetric analysis (TGA) was performed using a Perkin-Elmer Pyris 1 TGA equipped with Pyris Thermal Analysis 7.0 software. HSQ samples were placed in a Pt pan and heated in N_2 or 4% H_2:96% N_2 atmospheres from room temperature to 1100 °C at 10, 20, 50, and 100 °C/min.

X-ray Photoelectron Spectroscopy (XPS). A Kratos Axis Ultra instrument operating in energy spectrum mode at 210 W was used for XPS measurements. The base pressure and operating chamber pressure were maintained at $\leq 1 \times 10^{-7}$ Pa. A monochromatic Al Kα source was used to irradiate the samples, and the spectra were obtained with an electron takeoff angle of 90°. Wide survey spectra were collected using an elliptical spot with 2 mm and 1 mm major and minor axis lengths, respectively, and 160 eV pass energy with a step of 0.33 eV. Sample compositions were determined from the peaks of the survey spectra with subtracted linear background using the internal instrument values of relative sensitivity factor. Sample charging was minimized using an electron gun.

Material Characterization and Instrumentation. Photoluminescence (PL) spectra of a thin film of finely powdered **7** dropcoated onto optical grade quartz from a pentane suspension were evaluated

(51) "SiO_x" is viewed as a kinetically inert, amorphous material that converts to the thermodynamically favored nanocrystalline Si and SiO_2 upon thermal processing. See ref 30.
(52) Brook, M. B. *Silicon in Organic Organometallic and Polymer Chemistry*; John Wiley and Sons, Inc.: New York, 2000.
(53) Feher, F. J.; Budzichowski, T. A.; Blanski, R. L.; Weller, K. J.; Ziller, J. W. *Organometallics* **1991**, *10*, 2526.
(54) Feher, F.; Newman, D. A. *J. Am. Chem. Soc.* **1990**, *112*, 1931.
(55) Feher, F.; Newman, D. A.; Walzer, J. F. *J. Am. Chem. Soc.* **1989**, *111*, 1741.
(56) Feher, F. J.; Budzichowski, T. A.; Rahimian, K.; Ziller, J. W. *J. Am. Chem. Soc.* **1992**, *114*, 3859.
(57) Azinovic, D.; Cai, J.; Eggs, C.; Konig, H.; Marsmann, H. C.; Veprek, S. *J. Lumin.* **2002**, *97*, 40.
(58) Tour, J. M.; Pendalwar, S. L.; Cooper, J. P. *Chem. Mater.* **1990**, *2*, 647.
(59) Brook, M. A.; Ketelson, H. A. M.; Pelton, R. H.; Heng, Y.-M. *Chem. Mater.* **1996**, *8*, 2195.
(60) Arkles, B.; Berry, D. H.; Figge, L. K.; Composto, R. J.; Chiou, T.; Colazzo, H.; Wallace, W. E. *Sol−Gel Sci. Technol.* **1997**, *8*, 465.
(61) Yang, C.-C.; Chen, W.-C. *J. Mater. Chem.* **2002**, *12*, 1138.
(62) Hummel, J.; Endo, K.; Lee, W. W.; Mills, M.; Wang, S. Q. *Low-Dielectric Constant Materials V*; The Materials Research Society: Warrendale, PA, 1999; Vol. 565.

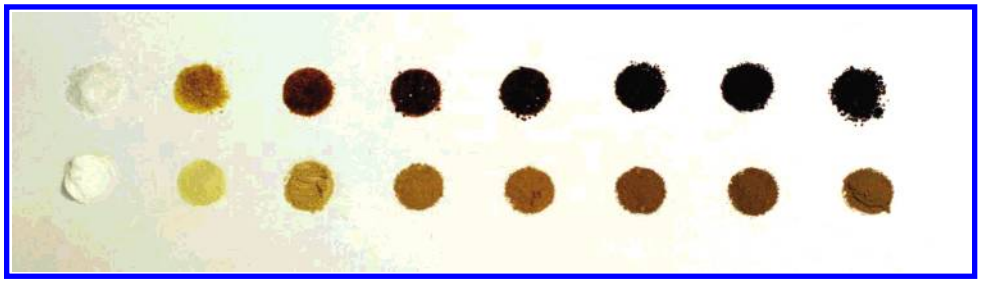

Figure 1. Photographs of HSQ and **1**−**7** (left to right), as prepared (top) and finely ground (bottom).

Table 1.

compd	processing temperature (°C)	color	yield (%)	nanocrystalline (yes/no)
1	500	orange	96	no
2	600	orange	95	no
3	700	orange/brown	94	no
4	800	orange/brown	94	no
5	900	brown/black	94	no
6	1000	brown/black	94	yes
7	1100	brown/black	94	yes
8	800, 1100	orange/brown, brown/black	94, 94	no, yes

Table 2.

compd	etch time[a] (min)	apparent PL color	PL maximum (nm)	quantum yield standard
9	30	N/A−partially etched	N/A	N/A
10	50	red	705	$[Ru(bpy)_3]Cl_2$
11	85	orange	612	$[Ru(bpy)_3]Cl_2$
12	115	yellow	585	rhodamine 590
13	135	green	512	fluorscein

[a] Etch times strongly depend on reagent concentrations and nanocomposite particle size.

at room temperature using the 325 nm line of a He−Cd laser excitation source and emission was detected with a fiber-optic digital charge-coupled device (CCD) spectrometer whose spectral response was normalized using a standard blackbody radiator. PL spectra of cloudy pentane solutions of **10**−**13** were obtained using a Cary Eclipse Fluorimeter. PL quantum yields were calculated by normalizing to appropriate standards.[63] Fourier-transform infrared spectroscopy (FT−IR) of pentane cast films of **7**, **9**, and **10**−**13** was performed using a Nicolet Magna 750 IR spectrophotometer. Transmission electron microscopy (TEM) and energy dispersive X-ray (EDX) analyses were preformed using a JEOL-2010 (LaB_6 filament) electron microscope with an accelerating voltage of 200 keV. Thin TEM samples of **7** were prepared by mounting a thin piece of material onto a copper grid with a 400 μm diameter hole. Samples were subsequently ion milled to perforation, and images were obtained from the edge of the milled hole. TEM samples of the liberated, freestanding Si nanoparticles were dropcoated from a pentane suspension onto carbon-coated copper grids. Bulk crystallinity of *nc*-Si/SiO_2 composites was evaluated using an INEL XRG 3000 X-ray diffractometer equipped with a Cu Kα radiation source.

3. Results and Discussion

Hydrogen silsesquioxane or HSQ is commercially available from Dow-Corning Corporation under the tradename FOx-(*XX*) where *XX* is a numeric notation describing the solution formulation (i.e., solvent and concentration). HSQ is currently marketed as a "flowable oxide" for use as a spin-on dielectric in the semiconductor industry. Here, we report that when HSQ is thermally processed in a 4% H_2:96%N_2 atmosphere, the white solid transforms into a dark glassy solid whose color and crystallinity depend on the peak processing temperature (Figure 1). TEM, SAED, XPS, and photoluminescence spectroscopy support XRD observations confirming that reductive thermal processing of HSQ at 1100 °C yields luminescent, diamond lattice, elemental silicon nanocrystallites encapsulated in an SiO_2-like matrix (vide infra). Matrix-embedded Si nanoparticles are readily liberated upon exposure to hydrofluoric acid solutions that preferentially etch away the SiO_2, leaving freestanding, highly luminescent *nc*-Si with emission maxima that are readily tuned throughout the visible region of the electromagnetic spectrum.[64]

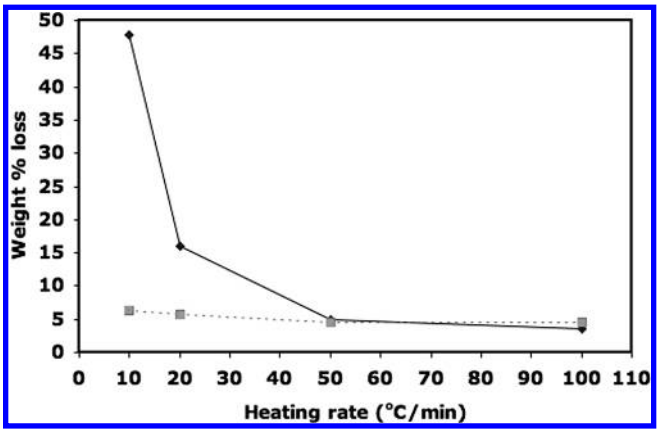

Figure 2. Heating rate dependence of HSQ weight loss. Solid, nitrogen atmosphere; dashed, 4% hydrogen and 96% nitrogen atmosphere.

Thermogravimetric Analysis. Thermal processing of HSQ was evaluated using thermogravimetric analysis (TGA). In a nitrogen atmosphere, thermal traces of HSQ obtained at a heating rate of 10 °C/min show four distinct regions of weight loss (ca. 50−225 °C, 1.8%; 225−375 °C, 2.1%; ca. 375−425 °C, 0.8%; ca. 507 °C, 43%). With increased heating rate (i.e., 10, 20, 50, and 100 °C/min), we note a dramatic decrease (Figure 2) in the observed weight loss at 507 °C (i.e., 10 °C/min, 43% vs 100 °C/min, 5%). TGA analysis of HSQ in 4%H_2:96%N_2 shows ca. 5% weight loss regardless of heating rate.

(63) Quantum yields were determined using the relationship $\phi_{SiNP} = \phi_r(A_r/A_{SiNP})(\eta_{SiNP}/\eta_r)(D_{SiNP}/D_r)$, where ϕ_{SiNP}, A_{SiNP}, η_{SiNP}, and D_{SiNP} are the quantum yields, absorbance at the excitation wavelength, refractive index, and integrated photoluminescence intensity, respectively. The corresponding terms with subscript "r" refer to equivalent parameters for the appropriate standard. For the present approximation, the following quantities were used: quantum yield (ϕ_r) of fluoroscein = 0.79, rhodamine 590 = 0.70, $[Ru(bpy)_3]Cl_2$ = 0.042, $\eta_{SiNP} \approx \eta_{pentane}$ = 1.357, $\eta_r \approx \eta_{water}$ = 1.333 for $[Ru(bpy)_3]Cl_2$, $\eta_r \approx \eta_{methanol}$ = 1.328 for fluorscein and rhodamine 590.

(64) Williams, K. R. *J. Microelectromech. Syst.* **1996**, *5*, No. 4.

Scheme 2. Stages of HSQ Thermal Degradation in an Inert Atmosphere

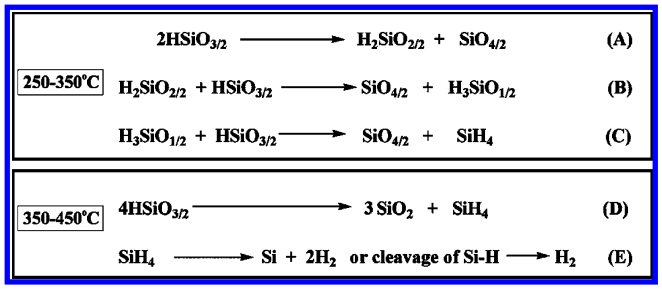

The accepted stages of HSQ thermal processing in an inert atmosphere (i.e., N_2 or Ar) are summarized in Scheme 2 and have previously been attributed to (i) trace solvent loss (<200 °C), (ii) cage network redistribution with associated loss of SiH_4 (ca. 250−350 °C), (iii) Si−H thermal dissociation accompanied by loss of SiH_4 and H_2 (350−450 °C), and (iv) collapse of the pore structure (>450 °C).[65] The structures of low-temperature (i.e., 250−350 °C) thermally processed HSQ thin films have been studied spectroscopically; however, the identity of any gas byproducts remains unknown. This is not the case for the high-temperature region of the TGA, for which the loss of SiH_4 and H_2 has been confirmed by mass spectrometry.[66] Consistent with our nitrogen atmosphere TGA observations, Belot et al. noted a decrease in SiH_4 evolution and weight loss at 507 °C with increased heating rates and proposed, in the absence of definitive evidence, that this resulted from the rapid thermal decomposition of SiH_4 into silicon and hydrogen.[66] Herein, we confirm that the observed trend in weight loss at ca. 450 °C, with increased heating rate, indeed results from the thermal decomposition of SiH_4 and the formation of amorphous clusters of elemental Si (vide infra). Upon rapid heating of HSQ (i.e., ≥50 °C/min under N_2 or ≥10 °C/min under 4% H_2:96% N_2), thermally liberated SiH_4 is unable to escape the rapidly forming silicon oxide matrix prior to decomposing.

Currently, the specific role of hydrogen in the thermal processing atmosphere is unclear and subject to further investigation in our laboratory. One possible explanation for the decreased weight loss may be H_2-induced modifications to the HSQ decomposition mechanism (Scheme 2E). It is conceivable that low H_2 concentrations in the thermal processing atmosphere limit and may even prevent the dehydrogenation of HSQ, thereby increasing the SiH_4 available for thermal decomposition.

X-ray Powder Diffraction (XRD). The crystallization of matrix-embedded *nc*-Si was evaluated by XRD (Figure 3). Analyses of composites **1**−**4** indicate that when HSQ is processed at temperatures below 800 °C, only a broad unassigned diffraction peak arising from the amorphous SiO_2-like matrix is observed and there are no characteristic reflections of diamond lattice Si. When HSQ is thermally processed at 900 °C (i.e., **5**), weak, very broad diffraction signals corresponding to the (220) and (311) reflections are discernible above the XRD baseline, indicating the formation of short-range crystalline order. The (220) and (311) peaks

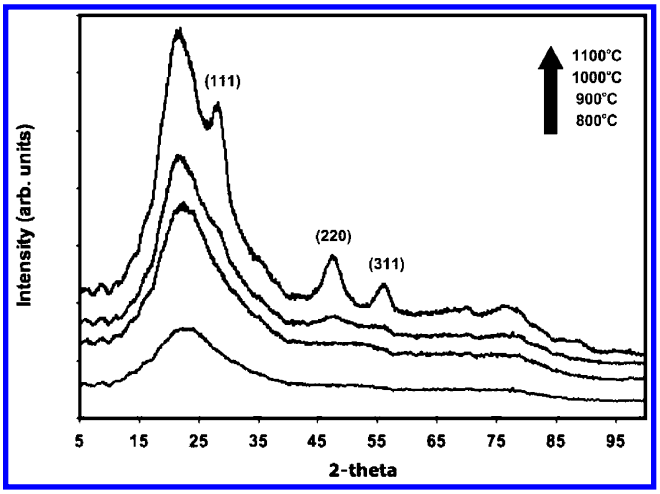

Figure 3. X-ray powder diffraction of composites **4**−**7** showing the peak thermal processing temperature dependence of Si nanodomain crystallinity. Characteristic (111), (220), and (311) reflections of the diamond lattice are noted.

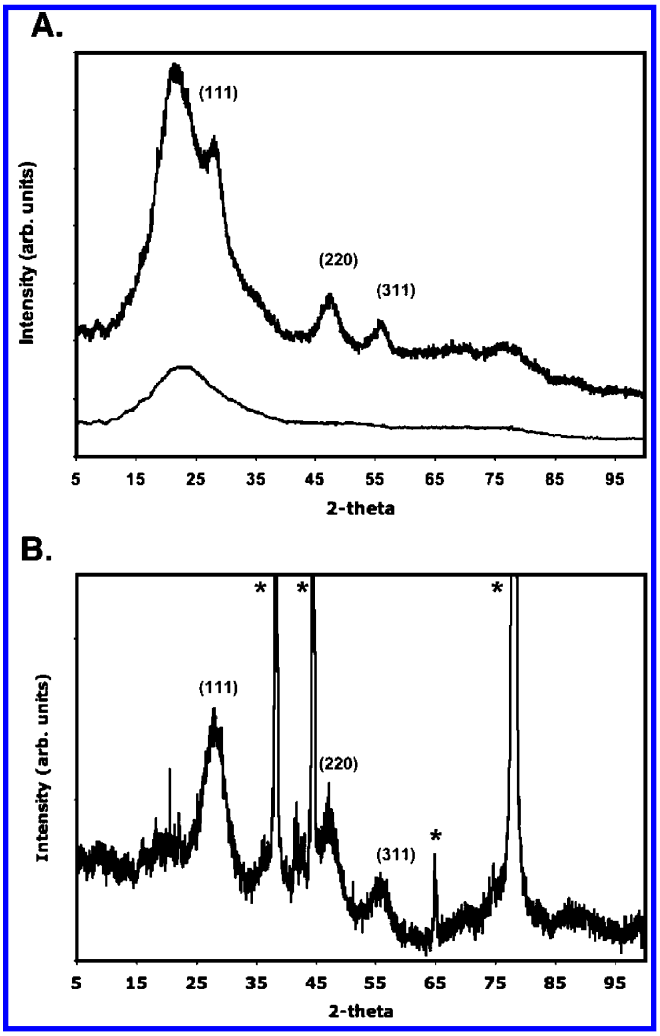

Figure 4. (A) X-ray powder diffraction of composites **4** (bottom) and **8** (top). Characteristic (111), (220), and (311) reflections of the diamond lattice are noted. (B) X-ray powder diffraction of **10**. Characteristic (111), (220), and (311) reflections of the diamond lattice and sample holder background peaks (∗) are noted.

(65) Detailed literature studies of HSQ thermal properties report on thermal processing of partially cross-linked HSQ gels and thin films, accounting for small differences in the present DSC temperature ranges. See: Yang, C.-C.; Chen, W.-C. *J. Mater. Chem.* **2002**, *12*, 1138.

(66) Belot, V.; Corriu, R.; Leclecq, D.; Mutin, P. H.; Vious, A. *Chem. Mater.* **1991**, *3*, 127.

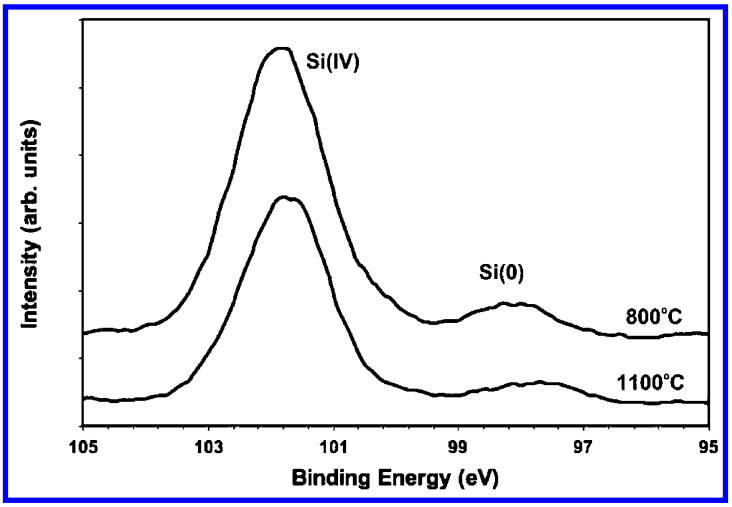

Figure 5. High-resolution X-ray photoelectron spectroscopy of the Si 2p spectral region of composites **4** (top) and **8** (bottom). Two emissions characteristic of SiO_2 and elemental silicon are noted for both samples independent of thermal processing temperature.

increase in intensity and narrow, whereas a characteristic (111) reflection becomes prominent for composites processed at higher temperatures (i.e., **6** and **7**). An estimated crystallite domain size of ca. 4 nm was obtained from the Scherrer relationship to the diffraction pattern obtained from **7**. The positions and intensities of all broadened reflections agree with selected area electron diffraction obtained for composite **7** and are consistent with diamond lattice Si. Samples thermally processed at lower temperatures (i.e., **1**−**4**) can be reprocessed at 1100 °C to produce similar nanocrystalline domains observed for composite **7** (Figure 4A). HF etching of **7** yields FS-*nc*-Si (vide infra). XRD patterns of the FS-*nc*-Si show no broad diffraction arising from the amorphous composite matrix, whereas the peaks characteristic of the diamond lattice Si remain (Figure 4B).

X-ray Photoelectron Spectroscopy. Survey XPS analyses of **2**−**8** confirm the presence of only silicon and oxygen. High-resolution scanning of the Si 2p region for composites **4**, **7**, and **8** show two peaks at approximately 101.9 and 98.1 eV, readily assigned to oxides of silicon and elemental silicon, respectively (Figure 5). The ratio of oxide and elemental Si 2p emission peaks is independent of the thermal-processing temperature, suggesting the formation of a constant amount of elemental Si regardless of thermal-processing temperature.

The TGA, XRD, and XPS data support a multistep thermal-decomposition mechanism that produces silicon nanocrystals. Thermal processing of HSQ produces silane. At rapid heating rates (e.g., ≥20 °C/min in 4% H_2), silane decomposes and yields noncrystalline clusters of elemental silicon that subsequently crystallize when heated above ca. 900 °C. Similar crystallization processes have been reported for SiO_X composites.[67]

FT−**IR Spectroscopy.** FT−IR spectroscopy of NEAT HSQ shows a characteristic absorption at 2251 cm^{-1} that is readily assigned to Si−H stretching (Figure 6A). Absorptions are also noted in the range of ca. 1300−800 cm^{-1} and have previously been assigned to internal vibrations of the Si−O−Si cage framework.[68] Following reductive thermal processing at or above 900 °C, the absorption arising from Si−H stretching disappears, suggesting that the HSQ molecules have cross-linked and the cage structure has collapsed (see Figure 6B). We also observe the replacement of broad HSQ Si−O−Si vibrations with a broad featureless absorption centered at ca. 1096 cm^{-1} that we assign to Si−O−Si bending in an SiO_2-like network. Figure 6C shows a typical FT−IR spectrum of a pentane cast film of **9**. Reappearance of the characteristic $Si-H_x$ stretching at 2100 cm^{-1} is consistent with at least partial hydride termination of the particles. Bending frequencies of the Si−O−Si bonding configuration at ≤1400 cm^{-1} remain a dominant spectral feature in this spectrum, indicating incomplete liberation. As expected, a marked decrease in the intensity of the Si−O−Si absorptions is noted with increased HF etching time. A representative FT−IR spectrum of fully etched, hydride-surface-terminated silicon particles (**12**) showing characteristic Si−H stretching and bending frequencies is shown in Figure 6D. A very weak Si−O−Si vibration is present in this spectrum and likely results from limited surface oxidation that occurs during sample preparation.[69] Weak C−H stretching and bending frequencies arising from residual pentane are also observed.

Photoluminescence Spectroscopy. HSQ shows no visible photoluminescence. Composites **1**−**7** exhibit no detectable photoluminescence upon exposure to a standard handheld UV light. However, excitation with the 325 nm line of a He−Cd laser yields characteristic *nc*-Si/SiO_2 emission at ca. 800 nm from a solid film of **7**. (Figure 7). Upon etching with an HF solution, silicon crystals are liberated from the oxide matrix and become highly luminescent. The emission maxima of these isolated nanocrystals depend on the etching time (Figure 8). The observed blue shift in PL maximum upon extended exposure to HF is consistent with previous reports for etched *nc*-Si/SiO_2 nanocomposites and can be attributed to quantum confinement effects arising from

(67) Wang, J.; Wang, X. F.; Li, Q.; Hryciw, A.; Meldrum, A. *Phil. Mag.* **2006**, in press.

(68) Albrecht, M. G.; Blanchette, C. *J. Electrochem. Soc.* **1998**, *145*, 4019.

(69) Etching times to achieve complete removal of the SiO_2-like matrix depend on the grinding efficiency of the composite material and the corresponding composite particle size.

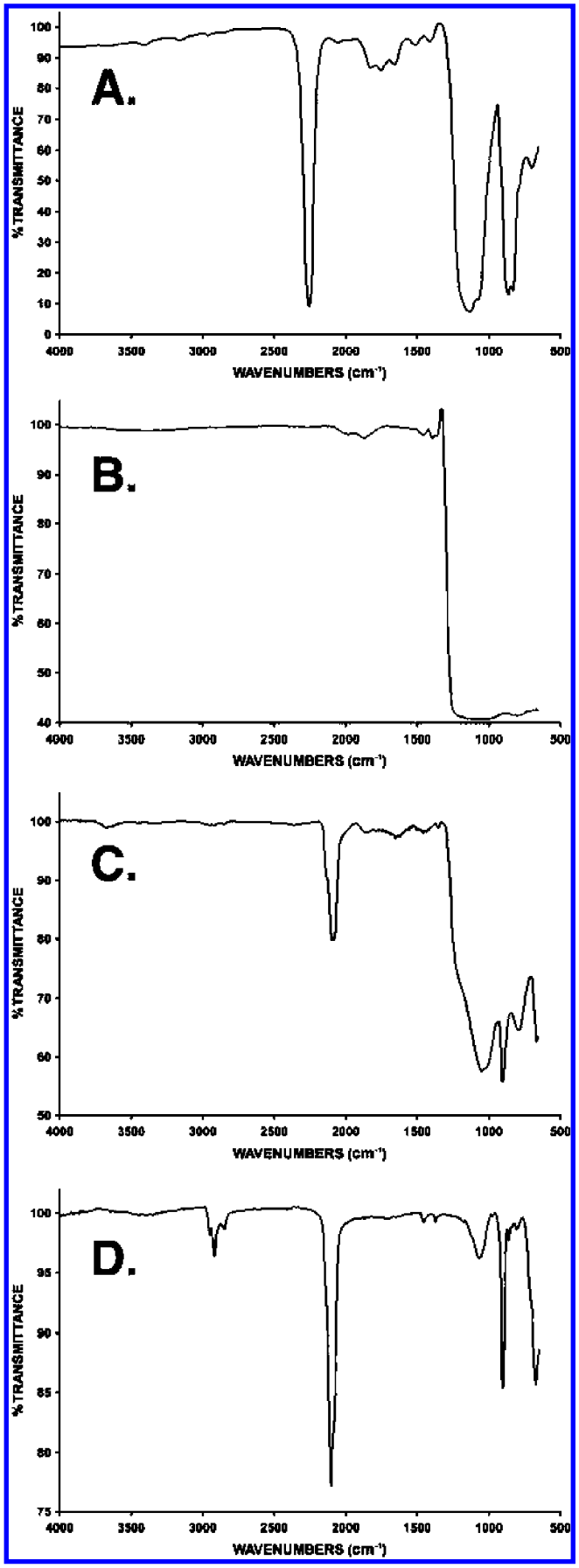

Figure 6. Infrared spectra of (A) NEAT hydrogen silsesquioxane and (B) NEAT **7**. HF etched annealed HSQ showing characteristic Si−H stretching (2100 cm^{-1}) and decreased Si−O−Si bending (1096 cm^{-1}) after (C) 30 min, **9**, and (D) 115 min, **12**.

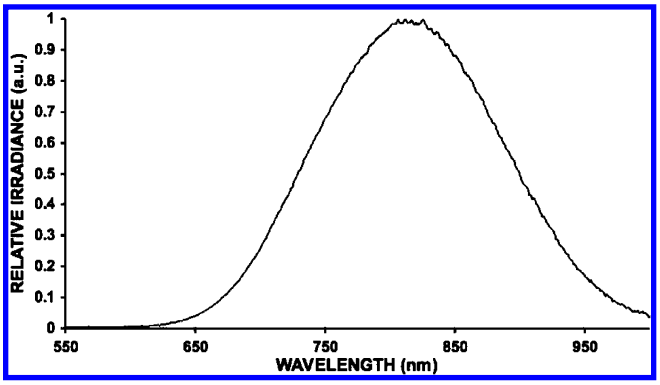

Figure 7. Photoluminescence spectrum obtained upon excitation of a thin film of **7** dropcoated from a pentane suspension of the finely ground powder onto optical grade silica using the 325 nm line of a He−Cd laser.

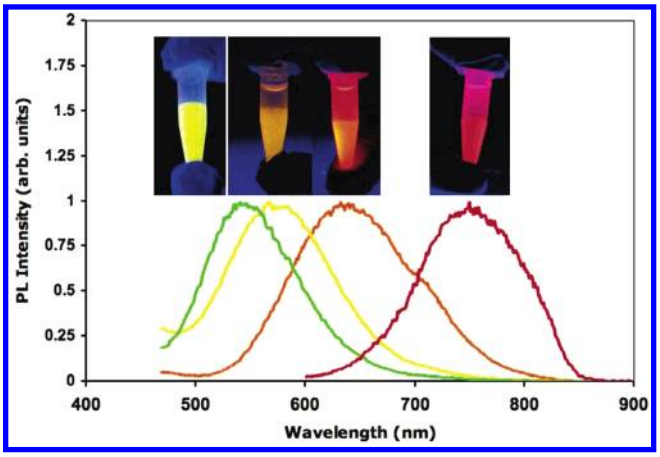

Figure 8. Photoluminescence spectra of pentane solutions of **10** (red), **11** (orange), **12** (yellow), and **13** (green). Inset: Photographs of photoluminescence observed from pentane suspensions of **10**−**13** upon exposure to a standard handheld UV light.

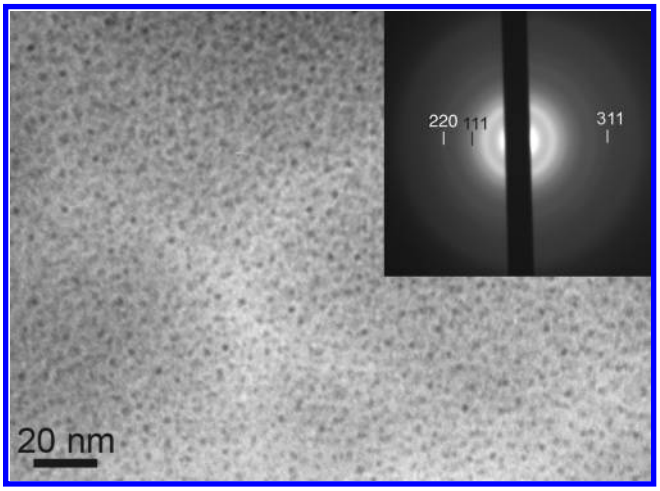

Figure 9. (A) Bright-field transmission electron micrograph of **7**. (Inset: Selected area electron diffraction of *nc*-Si/SiO_2 thin film composite showing (111), (200), and (311) reflections, characteristic of diamond lattice Si.)

decreased particles size. External photoluminescence quantum yields of isolated, hydride-surface-terminated Si particles are approximately 4%, consistent with those reported for similar systems in hydrocarbon solvents.[21,70] Still, light scattering from the characteristically cloudy solutions of hydride-terminated FS-*nc*-Si limit quantitative interpretation of this data.

(70) Fojtik, A.; Henglein, A. *J. Phys. Chem B* **2006**, *110*, 1994.

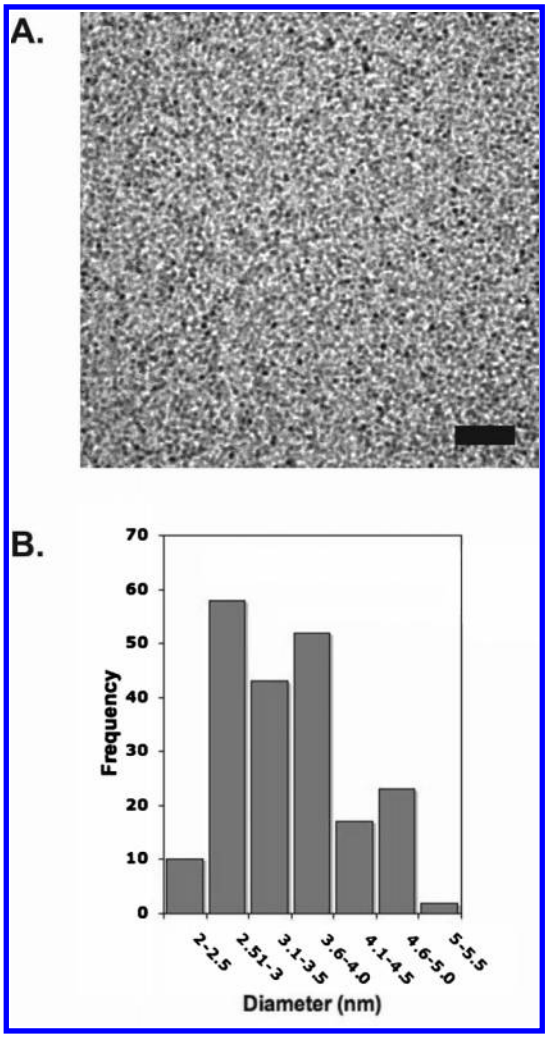

Figure 10. (A) Representative bright-field transmission electron micrograph of **12** (bar = 20 nm). (B) Size distribution of **12** providing average particle dimensions of $d = 3.41$ nm ($2\sigma = 1.40$ nm; $n = 188$).

Transmission Electron Microscopy, EDX, and SAED. Figure 9 shows a representative bright-field TEM image of a mounted piece of **7** that has been ion milled to perforation. This image shows irregular *nc*-Si particles. It can be concluded that silicon nanoparticles are uniformly distributed throughout the composite; however, no meaningful size or size distribution can be obtained from this image. EDX analysis confirms the presence of only Si and O. Selected area electron diffraction (Figure 9, inset) shows the particles are crystalline and have the characteristic diamond lattice of silicon, supporting present XRD analysis. TEM of HF-liberated *nc*-Si on carbon-coated grids show discrete Si nanoparticles with diameters of $d = 3.41$ nm ($2\sigma = 1.40$ nm; $n = 188$) and is consistent with Scherrer analysis of XRD signal broadening (Figure 10).

4. Conclusion

The present report outlines a straightforward method for preparing macroscopic quantities of *nc*-Si/SiO_2 and FS-*nc*-Si that luminesce in the visible and near-IR regions of the electromagnetic spectrum. Thermogravimetric analysis indicates that the sample heating rate and processing atmosphere influence the weight loss arising from SiH_4 evolution. Transmission electron microscopy, selected area electron diffraction, X-ray powder diffraction, and X-ray photoelectron spectroscopy all confirm the presence of *nc*-Si. In addition, the solution processability, ease of handling, and chemical tunability of silsesquioxanes will facilitate the preparation of patterned optoelectronic films with a tailored chemical response for incorporation into a variety of device structures, including chemical sensors, optical amplifiers, and waveguides.

Acknowledgment. C. Blois is thanked for assistance in obtaining the TEM micrographs. W. Moffat and Ryan Lister are thanked for assistance with TGA and FT−IR analyses. Angela Beltaos is thanked for technical assistance. Dr. A. Meldrum and J. Macdonald are thanked for useful discussions. The University of Alberta and NSERC are thanked for funding.

CM0602803